

# Generic Contrast Agents

Our portfolio is growing to serve you better. Now you have a *choice*.



[VIEW CATALOG](#)

# AJNR

This information is current as of May 29, 2025.

## **Diffusion Tractography Biomarkers of Pediatric Cerebellar Hypoplasia/Atrophy: Preliminary Results Using Constrained Spherical Deconvolution**






S. Fiori, A. Poretti, K. Pannek, R. Del Punta, R. Pasquariello, M. Tosetti, A. Guzzetta, S. Rose, G. Cioni and R. Battini

*AJNR Am J Neuroradiol* 2016, 37 (5) 917-923

doi: <https://doi.org/10.3174/ajnr.A4607>

<http://www.ajnr.org/content/37/5/917>

# Diffusion Tractography Biomarkers of Pediatric Cerebellar Hypoplasia/Atrophy: Preliminary Results Using Constrained Spherical Deconvolution

 S. Fiori,  A. Poretti,  K. Pannek,  R. Del Punta,  R. Pasquariello,  M. Tosetti,  A. Guzzetta, S. Rose,  G. Cioni, and  R. Battini



## ABSTRACT

**BACKGROUND AND PURPOSE:** Advances in MR imaging modeling have improved the feasibility of reconstructing crossing fibers, with increasing benefits in delineating angulated tracts such as cerebellar tracts by using tractography. We hypothesized that constrained spherical deconvolution–based probabilistic tractography could successfully reconstruct cerebellar tracts in children with cerebellar hypoplasia/atrophy and that diffusion scalars of the reconstructed tracts could differentiate pontocerebellar hypoplasia, nonprogressive cerebellar hypoplasia, and progressive cerebellar atrophy.

**MATERIALS AND METHODS:** Fifteen children with cerebellar ataxia and pontocerebellar hypoplasia, nonprogressive cerebellar hypoplasia or progressive cerebellar atrophy and 7 controls were included in this study. Cerebellar and corticospinal tracts were reconstructed by using constrained spherical deconvolution. Scalar measures (fractional anisotropy and mean, axial and radial diffusivity) were calculated. A general linear model was used to determine differences among groups for diffusion MR imaging scalar measures, and post hoc pair-wise comparisons were performed.

**RESULTS:** Cerebellar and corticospinal tracts were successfully reconstructed in all subjects. Significant differences in diffusion MR imaging scalars were found among groups, with fractional anisotropy explaining the highest variability. All groups with cerebellar pathologies showed lower fractional anisotropy compared with controls, with the exception of cerebellar hypoplasia.

**CONCLUSIONS:** This study shows the feasibility of constrained spherical deconvolution to reconstruct cerebellar and corticospinal tracts in children with morphologic cerebellar pathologies. In addition, the preliminary results show the potential utility of quantitative analysis of scalars of the cerebellar white matter tracts in children with cerebellar pathologies such as cerebellar hypoplasia and atrophy. Further studies with larger cohorts of patients are needed to validate the clinical significance of our preliminary results.

**ABBREVIATIONS:** AD = axial diffusivity; CA = progressive cerebellar atrophy; CH = nonprogressive cerebellar hypoplasia; CPCT = corticopontocerebellar tract; CST = corticospinal tract; CTT = cerebellar-thalamic tract; dMRI = diffusion MR imaging; FA = fractional anisotropy; MD = mean diffusivity; PCH = pontocerebellar hypoplasia; RD = radial diffusivity

In past years, there has been an increasing interest in the application of advanced MR imaging techniques for in vivo investigation of WM microstructure by using diffusion MR imaging (dMRI).<sup>1</sup> dMRI provides image contrast based on differences in the magnitude of diffusion of water molecules in the brain.<sup>2</sup> By combining the directional information and magnitude of anisotropic diffusion of the individual voxels, the trajectories of the


main WM tracts in the brain can be reconstructed<sup>2,3</sup> and quantitative analysis of WM organization can be performed.<sup>2</sup> dMRI scalars can be measured in specific anatomic ROIs or within/along reconstructed WM tracts to measure tissue properties.<sup>2</sup> Several studies have shown that advanced fiber tractography algorithms provide invaluable qualitative and quantitative information on the brain WM microstructure that cannot be obtained with conventional structural neuroimaging sequences.<sup>2,4</sup>


Developments in high-angular-resolution diffusion imaging<sup>5,6</sup> and progress in postprocessing software that take into ac-

Received July 24, 2015; accepted after revision September 29.

From Istituto di Ricovero e Cura a Carattere Scientifico Stella Maris Foundation (S.F., R.D.P., R.P., M.T., A.G., G.C., R.B.), Pisa, Italy; Section of Pediatric Neuroradiology (A.P.), Division of Pediatric Radiology, Russell H. Morgan Department of Radiology and Radiological Science, The Johns Hopkins School of Medicine, Baltimore, Maryland; Commonwealth Scientific and Industrial Research Organization (K.P., S.R.), Centre for Computational Informatics, Brisbane, Australia; Department of Computing (K.P.), Imperial College London, London, United Kingdom; and Department of Clinical and Experimental Medicine (A.G., G.C.), University of Pisa, Pisa, Italy.

Please address correspondence to Simona Fiori, MD, Department of Developmental Neuroscience, IRCCS Stella Maris Foundation, Viale Del Tirreno 331, 56128 Calambrone, Pisa, Italy; e-mail: s.fiori@fsm.unipi.it

 Indicates article with supplemental on-line table.

 Indicates article with supplemental on-line photo.

<http://dx.doi.org/10.3174/ajnr.A4607>

count multiple fiber orientations in the same voxel have improved the correct anatomic reconstruction of WM tracts such as the afferent and efferent cerebellar pathways<sup>5-9</sup> by accommodating crossing fibers. Improvements in fiber tractography of the cerebellar pathways are important because a large number of congenital, acquired, or degenerative diseases of pediatric<sup>10-26</sup> and adult<sup>27-31</sup> populations affect the cerebellum.

Currently, the diagnosis of nonprogressive cerebellar hypoplasia (CH) and progressive cerebellar atrophy (CA) is based on qualitative criteria that take into account conventional, structural MR imaging sequences.<sup>32-35</sup> CH refers to a developmental (nonprogressive) reduction of cerebellar volume with preserved near-normal shape,<sup>32</sup> while CA is defined as progressive loss of cerebellar parenchyma, with secondary enlargement of the interfolia space.<sup>33</sup> In some diseases with prenatal onset, hypoplasia of the cerebellum may be associated with pontine hypoplasia (ie, pontocerebellar hypoplasia [PCH]<sup>17</sup>). Despite improvement of structural MR imaging techniques (eg, phased array and higher magnetic field), differentiation of CH and CA remains challenging, particularly when only 1 MR imaging study is available.<sup>32-35</sup> A correct distinction between CH and CA is important in terms of management, prognosis, and family counseling. Neuroimaging methods that may increase the sensitivity in the diagnosis of CH and CA are warranted.

We aimed to study the feasibility of constraint spherical deconvolution fiber tractography to reconstruct cerebellar WM tracts and corticospinal tracts (CSTs) in children with PCH, CH, and CA. We hypothesized that despite different degrees of reduction of cerebellar volumes, our approach could successfully reconstruct cerebellar tracts. In addition, we aimed to measure microstructural properties of cerebellar tracts and CSTs in patients and age-matched controls. We expected that the reconstructed WM tracts would show altered scalar metrics in patients compared with controls. Differences in dMRI scalars of the cerebellar tracts and CSTs among the 3 groups of patients may shed light on the underlying pathomechanism causing macroscopic cerebellar abnormalities and may facilitate the differentiation among the 3 groups of diseases.

## MATERIALS AND METHODS

### Subjects

Children with cerebellar ataxia for this prospective study were recruited at Stella Maris Scientific Institute from June 2013 to January 2015 and underwent MR imaging as part of their clinical diagnostic work-up. Inclusion criteria for this study were evidence of isolated PCH, CH, or CA on structural conventional MR imaging and the availability of 2 structural MR imaging studies at least 1 year apart to clearly differentiate CH and CA. On the basis of the 2 structural neuroimaging studies, all patients were classified into the following groups: CH, PCH, and CA.<sup>32-35</sup> Children with supratentorial abnormalities were excluded from the study. Age-matched typically developing children were recruited as controls. The institutional review board approved the study, and informed parental consent was obtained for all participants.

### Data Acquisition

MR imaging data were acquired by using a 1.5T MR imaging scanner (Signa Horizon 1.5; GE Healthcare, Milwaukee, Wisconsin). A high-resolution structural 3D T1 BRAVO sequence (GE Healthcare) was acquired by using the following parameters: section thickness, 0.9 mm; FOV, 25.6 × 31.5 cm; TR/TE, 12.36/5.18 ms; flip angle, 13°. The acquisition time was 4 minutes and 30 seconds. dMRI data were acquired by using an echo-planar multidirection diffusion-weighted sequence. The imaging parameters were the following: 45 axial sections; section thickness, 3 mm; FOV, 24 × 29.6 cm; acquisition matrix, 80 × 80 (in-plane resolution, 3.0 × 3.7 mm); TR/TE, 11,000/92 ms. dMRI data were acquired along 30 noncollinear directions by using a b-value of 1000 s/mm<sup>2</sup>, in which the encoding gradients were distributed in space by using the electrostatic approach. In addition, 1 measurement without diffusion weighting (*b*=0 ss/mm<sup>2</sup>) was performed. The dMRI acquisition time was 6 minutes.

### Structural Image Analysis

Structural images were assessed by an experienced pediatric neuroradiologist (R.P.). All MR imaging studies were qualitatively evaluated for the presence of CH, PCH, or CA according to published diagnostic criteria.<sup>15,17</sup> Supratentorial structures were systematically assessed to exclude children with cerebral involvement.

### dMRI Data Analysis and Fiber Tractography

An extensive preprocessing procedure was performed to detect and correct image artifacts caused by involuntary head motion, cardiac pulsation, and intensity inhomogeneities, as previously described,<sup>23,36,37</sup> by using FSL tools (<http://www.fmrib.ox.ac.uk/fsl>),<sup>38</sup> ANTS (<http://picsl.upenn.edu/software/ants/>), and in-house tools. Constrained spherical deconvolution was used to estimate the fiber-orientation distribution for fiber tractography with the MRtrix package (<http://neuro.debian.net/pkgs/mrtrix.html>).<sup>6</sup> To facilitate manual ROI placement, we generated a short-track color-encoded track-density image by using 5 million streamlines of a maximum length of 2 cm seeded throughout the entire brain volume.<sup>23,36,37</sup> Cerebellar tracts were reconstructed on the basis of a multi-ROI approach (On-line Figure).

The corticopontocerebellar tract (CPCT) constitutes the main afferent pathway from the cerebral cortex to the cerebellum. To identify the CPCT, we placed a seeding ROI in the middle cerebellar peduncle (drawn on the coronal plane of the track-density image map in the green area [anteroposterior fiber direction]) and an inclusion ROI in the posterior limb of the internal capsule (drawn on the axial plane of the color-coded track-density image in the blue area [top-down fibers direction]). Frontal, parietal, and occipital projections to the cerebellum were included. ROIs were drawn separately for the right and left sides.

The cerebellar-thalamic tract (CTT) is the main efferent tract from the cerebellum. To identify the CTT, we placed a seeding ROI in the superior cerebellar peduncle (drawn on the coronal plane of the track-density image map in the light blue area [anteroposterior mixed with top-down fiber direction, more vertically displaced compared with CPCT]) separately on the right and left sides.

The CST originates from the precentral areas and descends through the centrum semiovale and ipsilateral posterior limb of internal capsule. To identify the CST, we chose the posterior limb of the internal capsule as the seeding ROI. An additional ROI was placed in the cerebral peduncle, on the right and left sides separately, on the axial plane of the color-coded track-density image, according to WM atlas mapping.<sup>3</sup>

Ten thousand streamlines were generated from the seeding ROIs. The maximum number of attempts (ie, number of seeded streamlines) was 1 million. Several exclusion ROIs were systematically placed to remove aberrant fibers.

Tracts were visually examined by 2 experienced raters (R.P. and S.F.) on all subjects to verify trajectory and anatomic landmarks described in the referenced atlas of human WM<sup>3</sup> and to check false-positive streamlines.

Fractional anisotropy (FA), mean diffusivity (MD), axial diffusivity (AD), and radial diffusivity (RD) were calculated as weighted mean values within each tract.

### Statistical Analysis

For all subjects, several dMRI scalars were calculated for each reconstructed tract. For each tract, a *t* test was used to compare dMRI scalars of the right and left sides. When no significant differences were found, the mean values of the right and left sides were averaged for further analysis.

A general linear model incorporating age as a covariate of no interest was used to determine the difference among groups for fiber tractography scalar measures (FA, MD, AD, RD). Post hoc pair-wise comparisons were performed to correct for multiple comparisons (Bonferroni-corrected *P* values).

Statistical analysis was performed by using SPSS, Version 2.0 (IBM, Armonk, New York), and all *P* values were 2-tailed. Results were considered significant at *P* < .05.

## RESULTS

### Subjects

Fifteen children (mean age,  $8.8 \pm 4.9$  years; range, 4–16 years) with cerebellar abnormalities and 7 normally developing controls (mean age,  $9.8 \pm 4.2$  years; range, 4–16 years) were recruited for this study. On the basis of structural MR imaging studies, patients were classified as follows: 5 children had CH (mean age,  $14.2 \pm 2.3$  years; range, 11–17 years), 5 patients had PCH (mean age,  $6.2 \pm 4.3$  years; range, 3–11 years), and 5 had CA (mean age,  $6.2 \pm 3.1$  years; range, 3–9 years). Detailed demographic, clinical, and genetic information of the 15 patients are shown in On-line Table 1.

Tracts were successfully reconstructed in all subjects (Fig 1); however, fewer than 10,000 streamlines were generated in all groups for both the CPCT (mean number,  $8050.89 \pm 2076.61$ ) and the CTT (mean number,  $5236.67 \pm 1731.02$ ), with no differences across groups or controls. No significant differences emerged in scalar measures between the right and left sides. Averaged means and SD of dMRI scalars for each tract are reported in Table 1. Results for FA and MD are plotted in Fig 2. All pair-wise comparisons for averaged scalar measures of each tract are reported in Table 2.

### Corticopontocerebellar Tract

There were significant differences among the groups in FA (*P* < .001,  $R^2 = 0.89$ ), MD (*P* = .005,  $R^2 = 0.59$ ), and RD (*P* = .001,  $R^2 = 0.71$ ). Post hoc analysis revealed that compared with controls, FA was reduced in PCH (Bonferroni-corrected *P* values < .001) and CA (Bonferroni-corrected *P* values = .002). PCH showed lower FA compared with CH (Bonferroni-corrected *P* values < .001) and CA (Bonferroni-corrected *P* values = .001). In addition, in PCH MD (Bonferroni-corrected *P* values = .005) and RD (Bonferroni-corrected *P* values < .001) values were higher compared with those of controls. No differences were found between controls and CH.

### Cerebellar-Thalamic Tract

There were significant differences between groups in FA (*P* < .001,  $R^2 = 0.80$ ) and RD (*P* = .014,  $R^2 = 0.49$ ). Post hoc analysis revealed that compared with controls, FA was significantly lower in PCH (Bonferroni-corrected *P* value < .001) and CA (Bonferroni-corrected *P* value < .001). PCH (Bonferroni-corrected *P* value = .001) and CA (Bonferroni-corrected *P* value = .019) showed lower FA compared with CH. Furthermore, PCH (Bonferroni-corrected *P* value = .041) and CA (Bonferroni-corrected *P* value = .028) showed higher RD compared with controls. No differences were detected between controls and CH.

### Corticospinal Tract

There were significant differences among groups in FA (*P* < .001,  $R^2 = 0.89$ ), AD (*P* = .003,  $R^2 = 0.56$ ), and RD (*P* < .001,  $R^2 = 0.75$ ). Post hoc analysis revealed that compared with controls, FA was lower in PCH (Bonferroni-corrected *P* value < .001) and CA (Bonferroni-corrected *P* value < .001). PCH showed lower FA compared with CH (Bonferroni-corrected *P* value < .001) and CA (Bonferroni-corrected *P* value = .041). Furthermore, PCH showed higher MD compared with controls (Bonferroni-corrected *P* value = .005) and higher RD compared with both controls (Bonferroni-corrected *P* value < .001) and CA (Bonferroni-corrected *P* value = .045). Finally, CA showed lower AD (Bonferroni-corrected *P* value = .043) compared with controls. No differences were detected between controls and CH.

## DISCUSSION

This study shows a 100% success rate for fiber tractography reconstruction of afferent (CPCT) and efferent (CTT) cerebellar tracts and the CST in children with CH, PCH, and CA. We used probabilistic tractography with constrained spherical deconvolution to reconstruct the WM tracts. In adults with ataxic syndromes, previous studies showed that probabilistic tractography is more accurate and less variable compared with deterministic tractography in reconstructing WM tracts within the cerebellar peduncles.<sup>31</sup> However, our very high successful rate is not straightforward because traditional tensor techniques have serious limitations in regions of crossing fibers due to the inability to represent multiple, independent intravoxel orientations. The superior cerebellar peduncles are the main component of the CTT and cross the midline in the midbrain at the level of the inferior colliculus. The dorsomedial portion of the superior cerebellar peduncle and its ventral fibers are the first to decussate, while the middle part de-



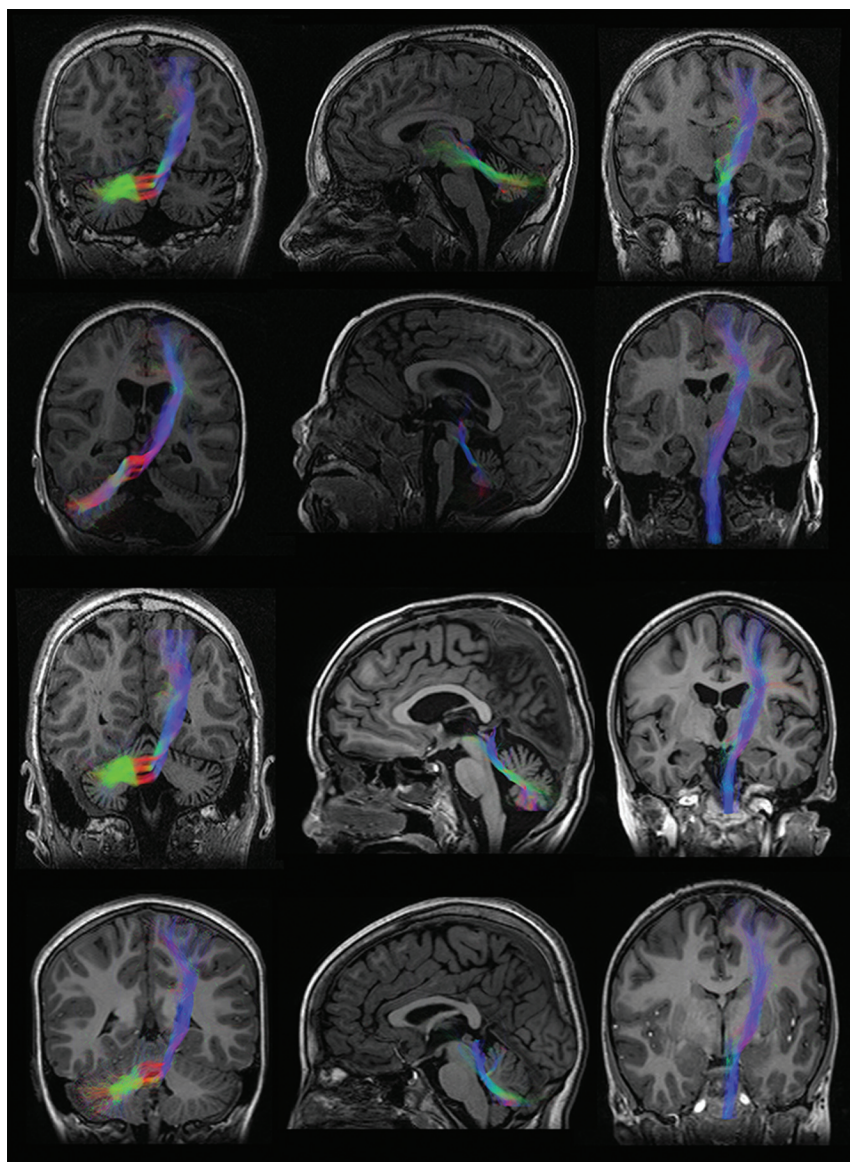


**FIG 1.** Reconstructed bundles for corticopontocerebellar (*left*), cerebellar-thalamic (*middle*), and corticospinal (*right*) tracts in subjects with (from *top to bottom*) CH, PCH, CA, and controls. Bundles are overlaid on T1-weighted images. Figures are representative of the global shape of the reconstructed bundles, irrespective of the cropping of the anatomic section.

**Table 1: Mean and SD of FA, MD, AD, and RD within the CPCT, CTT, and CST**

Tract/Group	FA Mean (SD)	MD Mean (SD) ( $10^{-3}$ mm <sup>2</sup> /s)	AD Mean (SD) ( $10^{-3}$ mm <sup>2</sup> /s)	RD Mean (SD) ( $10^{-3}$ mm <sup>2</sup> /s)
CPCT				
CH	0.42 (0.03)	0.98 (0.11)	1.42 (0.12)	0.76 (0.09)
PCH	0.27 (0.04)	1.14 (0.14)	1.41 (0.08)	0.99 (0.14)
CA	0.35 (0.03)	0.99 (0.03)	1.36 (0.03)	0.81 (0.04)
Control	0.44 (0.02)	0.88 (0.07)	1.37 (0.09)	0.66 (0.06)
CTT				
CH	0.28 (0.03)	1.39 (0.11)	1.79 (0.09)	1.26 (0.17)
PCH	0.19 (0.03)	1.49 (0.18)	1.79 (0.23)	1.39 (0.14)
CA	0.22 (0.02)	1.59 (0.14)	1.68 (0.21)	1.41 (0.15)
Control	0.29 (0.02)	1.29 (0.17)	1.81 (0.19)	1.27 (0.21)
CST				
CH	0.44 (0.02)	1.07 (0.29)	1.69 (0.16)	0.91 (0.11)
PCH	0.31 (0.03)	1.29 (0.13)	1.71 (0.19)	1.08 (0.11)
CA	0.36 (0.03)	1.06 (0.06)	1.46 (0.05)	0.86 (0.06)
Control	0.45 (0.02)	0.97 (0.04)	1.43 (0.06)	0.73 (0.04)

cussates at a more rostral level. The middle cerebellar peduncle represents the last portion of the CPCT. Middle cerebellar peduncles connect the brain stem nuclei with the contralateral cerebellar hemisphere and cross the midline at the level of the pons. Constrained spherical deconvolution is a new and innovative model of the diffusion signal that allows the resolution of crossing fibers in voxels containing multiple fiber orientations.<sup>6</sup> Compared with classic tensor models, it improves the estimated fiber orientations present in each voxel, which is especially important for fiber tractography of bundles with abundant crossing fibers, such as the cerebellar tracts, and allows a more accurate reconstruction of WM tracts.

High-order probabilistic fiber tractography models provide not only qualitative but also quantitative information, and dMRI scalars (FA, MD, AD, and RD) can be measured. The results of our study show differences in dMRI scalars of the cerebellar tracts and CST among the 3 groups of patients and controls. Our findings further support the high value of quantitative analysis of dMRI scalars to assess tissue microstructural properties in children with different cerebellar diseases.<sup>30,31</sup> dMRI scalars are derived from tensor eigenvalues and depend on WM characteristics such as axonal density and the size and degree of myelination.<sup>2,39,40</sup> AD describes water molecule mobility along the main fiber orientation axis (estimates axonal injury<sup>41</sup>), while RD describes water mobility perpendicular to the fiber axis (estimates myelin injury<sup>41</sup>). FA describes the relationship between AD and RD and is related to MD (eg, often a decrease in FA is associated with an increase in MD and RD). Each dMRI scalar, however, can be affected by different tissue properties.<sup>2</sup> In our study, FA values explained the highest amount of variability across groups, in agreement with previous studies.<sup>2,31,39,40</sup> MD changed consistently with FA as shown in Fig 2 but explained across-group variability to a lesser degree.

Post hoc analysis revealed differences in FA and RD values between children with cerebellar pathologies and controls, with the exception of patients with CH. Compared with controls, changes in MD reached statistical significance only in the

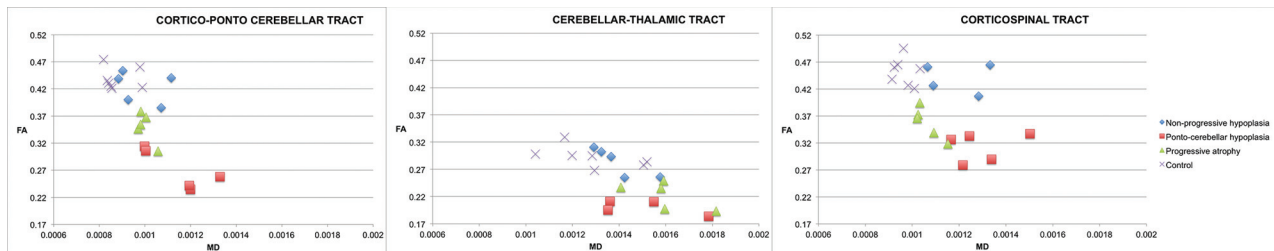


**FIG 2.** Plots of fractional anisotropy and mean diffusivity within the corticopontocerebellar, cerebellar-thalamic, and corticospinal tracts for CH, PCH, CA, and controls.

**Table 2: Pair-wise comparisons for averaged scalar measures of each tract**

	PCH	CA	Control
CPCT			
CH			
FA	(pB < .001) <sup>a</sup>	(pB = .242)	(pB = .714)
MD	(pB = 1.000)	(pB = 1.000)	(pB = .278)
AD	(pB = 1.000)	(pB = 1.000)	(pB = .297)
RD	(pB = .212)	(pB = 1.000)	(pB = .277)
PCH			
FA		(pB < 0.001) <sup>a</sup>	(pB < .001) <sup>a</sup>
MD		(pB = 0.149)	(pB = .005) <sup>a</sup>
AD		(pB = 1.000)	(pB = .952)
RD		(pB = .045) <sup>a</sup>	(pB < .001) <sup>a</sup>
CA			
FA			(pB = .002) <sup>a</sup>
MD			(pB = .821)
AD			(pB = 1.000)
RD			(pB = .289)
CTT			
CH			
FA	(pB = .001) <sup>a</sup>	(pB = .019) <sup>a</sup>	(pB = 1.000)
MD	(pB = 1.000)	(pB = 1.000)	(pB = 1.000)
AD	(pB = 1.000)	(pB = 1.000)	(pB = 1.000)
RD	(pB = 1.000)	(pB = 1.000)	(pB = .715)
PCH			
FA		(pB = .293)	(pB < .001) <sup>a</sup>
MD		(pB = 1.000)	(pB = .504)
AD		(pB = .914)	(pB = 1.000)
RD		(pB = 1.000)	(pB = .041) <sup>a</sup>
CA			
FA			(pB = .001) <sup>a</sup>
MD			(pB = .071)
AD			(pB = .315)
RD			(pB = .028) <sup>a</sup>
CST			
CH			
FA	(pB < .001) <sup>a</sup>	(pB = .082)	(pB = .492)
MD	(pB = .621)	(pB = 1.000)	(pB = 1.000)
AD	(pB = 1.000)	(pB = .289)	(pB = .143)
RD	(pB = .265)	(pB = 1.000)	(pB = .018)
PCH			
FA		(pB = .041) <sup>a</sup>	(pB < .001) <sup>a</sup>
MD		(pB = .221)	(pB = .005) <sup>a</sup>
AD		(pB = .040) <sup>a</sup>	(pB = .157)
RD		(pB = .045) <sup>a</sup>	(pB < .001) <sup>a</sup>
CA			
FA			(pB < .001) <sup>a</sup>
MD			(pB = 1.000)
AD			(pB = 1.000)
RD			(pB = .215)

**Note:**—pB indicates Bonferroni-corrected *P* value.

<sup>a</sup> Significant.

CPCT of children with PCH. However, boxplots showed a trend of changes in MD in children with CA matching FA changes across groups (reduction of FA corresponded to an increase of MD and RD<sup>2</sup>). Changes in dMRI scalars in cerebellar WM tracts may generally result from primary or secondary involvement. In WM tracts with primary involvement, myelin necrosis and axonal loss may lead to the formation of cystic spaces filled by CSF. The increased content of unhindered, isotropically diffusing water in these cavities is shown by a marked increase in MD.<sup>42</sup> On the contrary, in secondary WM involvement, there is neither substantial water accumulation in the interstitial spaces nor formation of cysts, even of microscopic dimensions, resulting in only a limited increase in MD.<sup>42</sup>

In children with PCH, we found a reduction of FA in all tracts compared with all groups, with the exception of CTT compared with children with CA. In addition, subjects with PCH showed higher MD and RD compared with controls in the CPCT and CST and higher RD in the CTT compared with controls. These findings support an involvement of WM tracts outside the cerebellum as previously shown by neuropathology studies.<sup>43</sup> In addition, neuropathology studies in PCH showed regressive (primary) changes with cystic formation in the cerebellar WM.<sup>44</sup> Degenerative cystic formation in the cerebellar WM causes an increase in isotropically diffusing water and, hence, a marked increase in MD as we found in the CPCT (including the middle cerebellar peduncle) of children with PCH. This explanation applies at least to 2 of the 5 patients with PCH. Three subjects with PCH had mutations in the *CASK* gene.<sup>45</sup> *CASK*-related PCH is rather of a malformative, not degenerative, nature. Neuropathology findings in a 2-week-old male patient revealed mainly GM involvement.<sup>46</sup> A more recent study, however, showed a role of *CASK* in axonal outgrowth and branching, supporting WM involvement as shown by our results.<sup>47</sup> Further studies including a larger and more homogeneous group of patients with PCH may elucidate the detailed pathomechanism leading to dMRI changes in GM or WM tracts within and outside of the cerebellum.

In children with CA, we found reduced FA compared with controls and CH in all reconstructed WM tracts and an increase in RD in the CTT, including the superior cerebellar peduncle. In neuronal ceroid lipofuscinosis and congenital disorders of glycosylation type 1a due to *PMM2* mutation, neuropathology studies showed that the primary involvement affected the cerebellar cortex with extensive loss of Purkinje cells and granule cells.<sup>48</sup> Neuropathology studies and our findings (decrease in FA and increase in RD without significant changes in MD) suggest that involvement of the cerebellar WM is most likely of a secondary nature

(Wallerian degeneration). In subjects with CA, we found dMRI changes not only within the cerebellar tracts but also in the CST. This finding may reflect a more diffuse involvement as shown in PCH. In neuronal ceroid lipofuscinosis, atrophy of the cerebral cortex and periventricular WM abnormalities have been reported.<sup>49</sup> Atrophy of the cerebral cortex and abnormalities of the subcortical WM have also been shown in congenital disorders of glycosylation type 1a.<sup>50</sup> Although no supratentorial abnormalities were detected in our patients on conventional MR imaging, changes in the CST may be secondary to ongoing injury of the cerebral cortex and subcortical WM.

In children with CH, we did not find differences in scalars compared with controls. This result is in contrast with the findings in CA and PCH. The lack of differences in dMRI scalars between children with CH and controls suggests that the microstructure of cerebellar WM tracts is preserved (eg, normal axonal packing, diameter, and myelination) and that a malformed cerebellum does not cause a secondary alteration of the connecting WM tracts (at least detectable by our approach). This finding is important for the primary or secondary role of the cerebellum in the pathogenesis of cognitive and affective impairment in children with CH. Distinction between CA and CH is not difficult in theory but can be problematic or impossible in practice on the basis of a single examination.<sup>32–35</sup> An accurate differentiation between CA and CH is important for a targeted diagnostic work-up, correct diagnosis, early institution of the correct therapy, prediction of the prognosis, and counseling of the family, including inheritance pattern and risk of recurrence. Our preliminary results suggest that FA values of the CTT may differentiate CA and CH on a single neuroimaging study. Our preliminary results, however, need to be validated in future studies, including larger cohorts of patients.

### Limitations

This study was performed in the context of a clinical MR imaging examination. Due to the need for a short acquisition time, we were able to apply only 30 gradient directions. This number of directions is too low to qualify the technique as high-angular-resolution diffusion imaging.<sup>5</sup> However, we believe that this number of directions is appropriate for a preliminary project to study the feasibility of advanced processing procedures with constrained spherical deconvolution in children with cerebellar pathologies. A higher number of gradient directions, measurement of DTI scalars along the white matter tracts (instead of 1 average value), and inclusion of additional white matter tracts (eg, spinocerebellar tracts) may provide additional important information and should be considered for future research studies, including a larger cohort of patients. The sample size is limited due to the inclusion criteria and the low prevalence of the included cerebellar pathologies in the pediatric population. However, the significant results, even in a small cohort of patients, are convincing.<sup>51</sup>

### CONCLUSIONS

Our study shows the feasibility of probabilistic tractography with constrained spherical deconvolution to reconstruct cerebellar tracts and the CST in children with morphologic cerebellar pathologies. In addition, our preliminary results show the potential

utility of quantitative analysis of scalars of the cerebellar WM tracts in children with cerebellar pathologies such as CH and CA. Further studies with larger cohorts of patients are needed to validate the clinical significance of our preliminary results.

### ACKNOWLEDGMENTS

We thank all children who took part in the study and their families.

### REFERENCES

- Assaf Y, Pasternak O. Diffusion tensor imaging (DTI)-based white matter mapping in brain research: a review. *J Mol Neurosci* 2008;34: 51–61 CrossRef Medline
- Jones DK, Knösche TR, Turner R. White matter integrity, fiber count, and other fallacies: the do's and don'ts of diffusion MRI. *Neuroimage* 2013;73:239–54 CrossRef Medline
- Mori S, Wakana S, Nagae-Poetscher LM, et al. *MRI Atlas of Human White Matter*. Amsterdam: Elsevier; 2005
- Rollins NK. Clinical applications of diffusion tensor imaging and tractography in children. *Pediatr Radiol* 2007;37:769–80 CrossRef Medline
- Tournier JD, Calamante F, Connelly A. Determination of the appropriate b value and number of gradient directions for high-angular-resolution diffusion-weighted imaging. *NMR Biomed* 2013;26: 1775–86 CrossRef Medline
- Tournier JD, Yeh CH, Calamante F, et al. Resolving crossing fibers using constrained spherical deconvolution: validation using diffusion-weighted imaging phantom data. *Neuroimage* 2008;42:617–25 CrossRef Medline
- Palesi F, Tournier JD, Calamante F, et al. Contralateral cerebello-thalamo-cortical pathways with prominent involvement of associative areas in humans in-vivo. *Brain Struct Funct* 2015;220: 3369–84 CrossRef Medline
- Chokshi FH, Poretti A, Meoded A, et al. Normal and abnormal development of the cerebellum and brainstem as depicted by diffusion tensor imaging. *Semin Ultrasound CT MR* 2011;32:539–54 CrossRef Medline
- Kamali A, Kramer LA, Frye RE, et al. Diffusion tensor tractography of the human brain cortico-ponto-cerebellar pathways: a quantitative preliminary study. *J Magn Reson Imaging* 2010;32:809–17 CrossRef Medline
- Klingberg T, Vaidya CJ, Gabrieli JD, et al. Myelination and organization of the frontal white matter in children: a diffusion tensor MRI study. *Neuroreport* 1999;10:2817–21 CrossRef Medline
- Saksena S, Husain N, Malik GK, et al. Comparative evaluation of the cerebral and cerebellar white matter development in pediatric age group using quantitative diffusion tensor imaging. *Cerebellum* 2008;7:392–400 CrossRef Medline
- Leitner Y, Travis KE, Ben-Shachar M, et al. Tract profiles of the cerebellar white matter pathways in children and adolescents. *Cerebellum* 2015 Feb 4. [Epub ahead of print] CrossRef Medline
- Boltshauser E. Cerebellar imaging: an important signpost in paediatric neurology. *Childs Nerv Syst* 2001;17:211–16 CrossRef Medline
- Poretti A, Huisman TA, Scheer I, et al. Joubert syndrome and related disorders: spectrum of neuroimaging findings in 75 patients. *AJNR Am J Neuroradiol* 2011;32:1459–63 CrossRef Medline
- Volpe JJ. Brain injury in premature infants: a complex amalgam of destructive and developmental disturbances. *Lancet Neurol* 2009;8: 110–24 CrossRef Medline
- Namavar Y, Barth PG, Kasher PR, et al. Clinical, neuroradiological and genetic findings in pontocerebellar hypoplasia. *Brain* 2011;134: 143–56 CrossRef Medline
- Widjaja E, Blaser S, Raybaud C. Diffusion tensor imaging of midline posterior fossa malformations. *Pediatr Radiol* 2006;36:510–17 CrossRef Medline
- Huisman TA, Bosemani T, Poretti A. Diffusion tensor imaging for



- brain malformations: does it help? *Neuroimaging Clin N Am* 2014; 24:619–37 CrossRef Medline
19. Bucci M, Mandelli ML, Berman JI, et al. Quantifying diffusion MRI tractography of the corticospinal tract in brain tumors with deterministic and probabilistic methods. *Neuroimage Clin* 2013;3: 361–68 CrossRef Medline
20. Poretti A, Boltshauser E, Loenneker T, et al. Diffusion tensor imaging in Joubert syndrome. *AJNR Am J Neuroradiol* 2007;28:1929–33 CrossRef Medline
21. Fiori S, Pannek K, Pasquariello R, et al. Corticopontocerebellar connectivity disruption in congenital hemiplegia. *Neurorehabil Neural Repair* 2015;29:858–66 CrossRef Medline
22. Law N, Bouffet E, Laughlin S, et al. Cerebello-thalamo-cerebral connections in pediatric brain tumor patients: impact on working memory. *Neuroimage* 2011;56:2238–48 CrossRef Medline
23. Jeong JW, Asano E, Juhász C, et al. Quantification of primary motor pathways using diffusion MRI tractography and its application to predict postoperative motor deficits in children with focal epilepsy. *Hum Brain Mapp* 2014;35:3216–26 CrossRef Medline
24. Lui YW, Law M, Chacko-Mathew J, et al. Brainstem corticospinal tract diffusion tensor imaging in patients with primary posterior fossa neoplasms stratified by tumor type: a study of association with motor weakness and outcome. *Neurosurgery* 2007;61:1199–1207; discussion 1207–08 CrossRef Medline
25. Kovanlikaya I, Firat Z, Kovanlikaya A, et al. Assessment of the corticospinal tract alterations before and after resection of brainstem lesions using diffusion tensor imaging (DTI) and tractography at 3T. *Eur J Radiol* 2011;77:383–91 CrossRef Medline
26. Law N, Greenberg M, Bouffet E, et al. Visualization and segmentation of reciprocal cerebrocerebellar pathways in the healthy and injured brain. *Hum Brain Mapp* 2015;36:2615–28 CrossRef Medline
27. Rizzo G, Tonon C, Valentino ML, et al. Brain diffusion-weighted imaging in Friedreich's ataxia. *Mov Disord* 2011;26:705–12 CrossRef Medline
28. Pagani E, Ginestroni A, Della Nave R, et al. Assessment of brain white matter fiber bundle atrophy in patients with Friedreich ataxia. *Radiology* 2010;255:882–89 CrossRef Medline
29. Ying SH, Landman BA, Chowdhury S, et al. Orthogonal diffusion-weighted MRI measures distinguish region-specific degeneration in cerebellar ataxia subtypes. *J Neurol* 2009;256:1939–42 CrossRef Medline
30. Yoon B, Kim JS, Lee KS, et al. Early pathological changes in the cerebellum of patients with pure cerebellar syndrome demonstrated by diffusion-tensor imaging. *Eur Neurol* 2006;56:166–71 CrossRef Medline
31. Prakash N, Hageman N, Hua X, et al. Patterns of fractional anisotropy changes in white matter of cerebellar peduncles distinguish spinocerebellar ataxia-1 from multiple system atrophy and other ataxia syndromes. *Neuroimage* 2009;47(suppl 2):T72–81 CrossRef Medline
32. Poretti A, Boltshauser E, Doherty D. Cerebellar hypoplasia: differential diagnosis and diagnostic approach. *Am J Med Genet C Semin Med Genet* 2014;166C:211–26 CrossRef Medline
33. Poretti A, Wolf NI, Boltshauser E. Differential diagnosis of cerebellar atrophy in childhood. *Eur J Paediatr Neurol* 2008;12:155–67 CrossRef Medline
34. Boltshauser E. Cerebellar hypoplasias. *Handb Clin Neurol* 2008;87: 115–27 CrossRef Medline
35. Boltshauser E. Cerebellum-small brain but large confusion: a review of selected cerebellar malformations and disruptions. *Am J Med Genet A* 2004;126A:376–85 CrossRef Medline
36. Pannek K, Raffelt D, Bell C, et al. HOMOR: higher order model outlier rejection for high b-value MR diffusion data. *Neuroimage* 2012;63:835–42 CrossRef Medline
37. Pannek K, Boyd RN, Fiori S, et al. Assessment of the structural brain network reveals altered connectivity in children with unilateral cerebral palsy due to periventricular white matter lesions. *Neuroimage Clin* 2014;5:84–92 CrossRef Medline
38. Jenkinson M, Beckmann CF, Behrens TE, et al. FSL. *Neuroimage* 2012;62:782–90 CrossRef Medline
39. Kanai R, Rees G. The structural basis of inter-individual differences in human behaviour and cognition. *Nat Rev Neurosci* 2011;12: 231–42 CrossRef Medline
40. Johansen-Berg H. Behavioural relevance of variation in white matter microstructure. *Curr Opin Neurol* 2010;23:351–58 CrossRef Medline
41. Song SK, Sun SW, Ramsbottom MJ, et al. Demyelination revealed through MRI as increased radial (but unchanged axial) diffusion of water. *Neuroimage* 2002;17:1429–36 CrossRef Medline
42. Pierpaoli C, Barnett A, Pajevic S, et al. Water diffusion changes in Wallerian degeneration and their dependence on white matter architecture. *Neuroimage* 2001;13:1174–85 Medline
43. Namavar Y, Barth PG, Poll-The BT, et al. Classification, diagnosis and potential mechanisms in pontocerebellar hypoplasia. *Orphanet J Rare Dis* 2011;6:50 CrossRef Medline
44. Barth PG, Aronica E, de Vries L, et al. Pontocerebellar hypoplasia type 2: a neuropathological update. *Acta Neuropathol* 2007;114: 373–86 CrossRef Medline
45. Takanashi J, Arai H, Nabatame S, et al. Neuroradiologic features of CASK mutations. *AJNR Am J Neuroradiol* 2010;31:1619–22 CrossRef Medline
46. Najm J, Horn D, Wimplinger I, et al. Mutations of CASK cause an X-linked brain malformation phenotype with microcephaly and hypoplasia of the brainstem and cerebellum. *Nat Genet* 2008;40: 1065–67 CrossRef Medline
47. Kuo TY, Hong CJ, Chien HL, et al. X-linked mental retardation gene CASK interacts with Bcl11A/CTIP1 and regulates axon branching and outgrowth. *J Neurosci Res* 2010;15:88:2364–73 CrossRef Medline
48. Anderson GW, Goebel HH, Simonati A. Human pathology in NCL. *Biochim Biophys Acta* 2013;1832:1807–26 CrossRef Medline
49. Jadav RH, Sinha S, Yasha TC, et al. Magnetic resonance imaging in neuronal ceroid lipofuscinosis and its subtypes. *Neuroradiol J* 2012; 25:755–61 CrossRef Medline
50. Feraco P, Mirabelli-Badenier M, Severino M, et al. The shrunken, bright cerebellum: a characteristic MRI finding in congenital disorders of glycosylation type 1a. *AJNR Am J Neuroradiol* 2012;33: 2062–67 CrossRef Medline
51. Friston K. Ten ironic rules for non-statistical reviewers. *Neuroimage* 2012;61:1300–10 CrossRef Medline